Assessment of sorption capability of montmorillonite clay for lead removal from water using laser–induced breakdown spectroscopy and atomic absorption spectroscopy

E.J. Terán, M.L. Montes, C. Rodríguez, L. Martino, M. Quiroga, R. Landa, R.M. Torres Sánchez, D.M. Díaz Pace

PII: S0026-265X(18)30839-7
DOI: doi:10.1016/j.microc.2018.08.047
Reference: MICROC 3331

To appear in: *Microchemical Journal*

Received date: 6 July 2018
Revised date: 23 August 2018
Accepted date: 24 August 2018

Please cite this article as: E.J. Terán, M.L. Montes, C. Rodríguez, L. Martino, M. Quiroga, R. Landa, R.M. Torres Sánchez, D.M. Díaz Pace , Assessment of sorption capability of montmorillonite clay for lead removal from water using laser–induced breakdown spectroscopy and atomic absorption spectroscopy. Microc (2018), doi:10.1016/j.microc.2018.08.047

Assessment of sorption capability of montmorillonite clay for Lead removal from water using laser–induced breakdown spectroscopy and atomic absorption spectroscopy

*E.J. Terán[a], M.L. Montes[b], C. Rodríguez[c], L. Martino[a], M. Quiroga[d], R. Landa[d], R.M. Torres Sánchez[e], D.M. Díaz Pace[a,]**

[a] *Centro de Investigaciones en Física e Ingeniería del Centro de la Provincia de Buenos Aires (CIFICEN), CONICET, CICPBA, Facultad de Ciencias Exactas UNCPBA, Campus Universitario, (B7000GHG) Tandil, Buenos Aires, Argentina.*

[b] *Instituto de Física La Plata (IFLP), CONICET, Departamento de Física, Facultad de Ciencias Exactas UNLP. 49 y 115, (7000) La Plata, Argentina.*

[c] *Centro de Investigaciones y Estudios Ambientales (CINEA). Facultad de Ciencias Humanas, UNCPBA. Campus Universitario, (B7000GHG) Tandil, Buenos Aires, Argentina.*

[d] *Centro de Investigación Veterinaria Tandil (CIVETAN), CONICET, CICPBA, Facultad de Ciencias Veterinarias UNCPBA, Campus Universitario, (B7000GHG) Tandil, Buenos Aires, Argentina.*

[e] *Centro de Tecnología de recursos Minerales y Cerámica (CETMIC), CONICET, CICPBA, Camino Centenario y 506, (B1897ZCA) Gonnet, Argentina.*

Abstract

Laser–induced breakdown spectroscopy (LIBS) and atomic absorption spectroscopy (AAS) techniques were applied for quantitative analysis of the remaining Pb content in water samples after treatment with a raw montmorillonite (MMT) and an organic derivative (MMO) clays for heavy metal removal, an issue of crucial importance for decontamination of water bodies. The Pb sorption capabilities of MMT and MMO clays were assessed by using solutions with known Pb concentrations, in the range 100–500 ppm. To carry out the LIBS analysis, the samples were prepared in the form of solid pellets with powdered calcium hydroxide addition. The measurement conditions were optimized to achieve reliable analytical results and the plasma parameters, i.e., temperature and electron density, were obtained. For quantification purpose, a calibration curve was constructed with the Pb I emission line at 4057.8 Å measured at the time window 30–45 μs by using reference samples with Pb concentrations in the range 56–715 ppm. The Pb residual content in the liquid samples determined with LIBS showed a good agreement with those measured with AAS. The sorption efficiency of Pb from contaminated water was calculated through a sorption percentage S_{Pb}%. The calculated S_{Pb}% was higher for MMT (56%–100%) than for MMO (27%–47%). The results also demonstrated the usefulness of LIBS method for the determination of Pb concentrations in liquid samples.

Key words: Pb; Montmorillonite; LIBS; AAS; Water; Decontamination.

*Corresponding author. E–mail address: *ddiaz@exa.unicen.edu.ar*
Tel.: +54–249 4439660/1. Fax: +54–249 4439669.
Postal address: Pinto 399, (B7000GHG) Tandil, Buenos Aires, Argentina.

1. Introduction

Pollution of natural ecosystems is a critical concern in medium– to large–sized urban areas worldwide due to it can affect the environmental quality and, then, the human health. This issue is particularly worse in less developed countries as a consequence of the high cost of the treatment technologies and the lack of proper regulations. In underdeveloped countries, the residues derived from industrial activities, which can contain heavy metals and others hazardous elements, are often released directly into the environment without a proper treatment. Once in the environment, they are dispersed through air, soils and surface water. Heavy metals are especially harmful due to their features of high toxicity, persistence, and accumulation. In fact, they were bio–accumulated in the food chain components, in a procedure known as bio–magnification, thus entailing a serious threat for human health and living organisms [1]. Therefore, monitoring heavy metal pollution in the environment is an issue of paramount importance as well as the development and investigation of new low-cost technologies aimed at advancing suitable strategies of remediation or mitigation of already affected sites. Particularly, water bodies are the most contaminated resources as a consequence of wastewater spills from activities related to industry, agriculture, and domestic sewage [2]. Hence, the environmental quality and the availability of water for human consumption, and other uses such as crops irrigation, may be considerably reduced due to the growth of metal concentrations present in environmental water respect to their natural levels.

Pb is a non–essential highly prevalent heavy metal which is usually found in the environment at trace levels. Pb concentration is increased respect to those guide values as a result of untreated spills from the manufacture of a widespread range of products, including batteries, paper, combustibles, printers, and paints, as well as waste from foundries and vehicles and factories emissions. Body tissues poisoning associated with human exposure to high levels of Pb, termed ‘saturnism’, is known a major cause of several adverse effects to brain, blood, bones, kidneys, and also to nervous, cardiovascular, and reproductive systems [3].

Different methods have been developed for the removal of hazardous elements from contaminated water. Among them, adsorption approaches have attracted much attention because they can employ low–cost environmental–friendly materials, such as natural clay minerals, that can sorb pollutants present in the water. The 2:1 clay mineral montmorillonite (MMT) has been studied driven by its potential application for removal of heavy metals from contaminated water bodies [4, 5]. MMT clay has several advantageous features respect to other cheap clays, such as availability, relatively high cation exchange capacity and specific surface area, which allows attaining high cationic species adsorption. Also the feasibility to modify its structure, which despite decreasing its adsorption capacity improve manipulation and easing recuperation as was shown for cationic fungicides [6]. In this scenario, laboratory studies are needed to further investigate MMT properties for heavy metal sorption aimed at decontamination of polluted water.

The major analytical laboratory methods employed for trace analysis are electro thermal atomization–atomic absorption spectroscopy (ETA–AAS), inductively coupled plasma–atomic emission spectroscopy (ICP–AES), and inductively coupled plasma–mass spectroscopy (ICP–MS) [7]. These methods are routinely employed for the analysis of trace elements in liquids sampled in environmental, industrial, pharmaceutical, and biological studies. However, they have the disadvantage that they are relatively expensive and time consuming because they require a laborious preparation of the samples. Over the past years, laser–Induced Breakdown Spectroscopy (LIBS) has emerged and established as a useful analytical technology to complement the conventional techniques thanks to its powerful attributes in terms of simplicity and versatility in applications to perform rapid, multi–element measurements with a minimum of sample preparation [8]. LIBS is an optical technique for qualitative and quantitative elemental analysis of solid, liquid, and gaseous samples based on the spectral analysis of the radiation emitted by a laser–induced plasma [9–11]. LIBS foundations lies on the generation of

a plasma with the material ablated from the target which emits characteristic spectral lines in the UV–Vis spectral range (200–900 Å). The physics of plasma generation and its temporal evolution are described in detail elsewhere [12]. Typical detection limits for LIBS are in the ppm range. Generally, obtaining qualitative results do not present major problems and the elements present in the sample are identified by their "chemical fingerprints". In contrast, carrying out a quantitative analysis is not straightforward because the emission intensity of a specie in the plasma is related to its elemental concentration and, also, to the experimental conditions under which it was generated, i.e., laser parameters, sample features, and surrounding atmosphere [13]. Typically, a stoichiometric ablation, i.e., the plasma composition is representative of that of the sample previous to the laser ablation, and local thermodynamic equilibrium (LTE) conditions are assumed.

The most common approach to achieve quantitative LIBS results is the construction of calibration curves employing matrix–matched standards. Nevertheless, the LIBS advantages do not come without limitations. The analysis is usually hampered by a number of difficulties present in applications performed in air at atmospheric pressure: transient plasma evolution, spatial inhomogeneity of the plume, and self–absorption of the spectral lines [14]. These issues affect adversely the accuracy of the LIBS results. Recent reviews by Hahn et al. [15,16] and Harmon et al. [17] summarized the current state–of–the–art on LIBS capabilities to analyze heavy metals on environmental liquid samples. On this regard, it is well known that the analysis of liquid samples by laser–produced plasmas generated in either the bulk or the surface has a number of drawbacks that worsen its analytical performance respect to solid samples, namely, splashing, bubbles, surface ripples, lower emitted intensity, and a shorter plasma life–time [18–20]. To overcome these difficulties, a number of researches addressed a liquid–to–solid sample transformation via different approaches. For instance, there have been used freezing samples [21, 22], surface liquid layers evaporated onto a substrate [23], evaporative pre–concentration inside salt water droplets [24], and laser–pretreated aluminum substrates [25]. In a previous work of our research group, liquid samples were converted into pellets of calcium hydroxide by mixing with calcium oxide [26]. In this process, the analytes resulted uniformly distributed inside the solid matrix and the advantages of direct interrogation of solids were accomplished.

On these steps, the goal of this work was to study of MMT sorption properties of Pb. To this aim, LIBS technique was applied for quantitative determination of the remaining Pb content in liquid solutions previously treated with MMT and organic MMT clays to assess its efficiency for Pb removal from water. Optimal experimental conditions were studied for improving the LIBS measurements. The Pb concentrations in the analytical solutions were crosschecked with the standard method atomic absorption spectroscopy (AAS).

2. Materials and methods

2.1 Samples and measurements

The samples used for Pb determination were liquid solutions derived from the Pb sorption experiments using raw Argentine montmorillonite (MMT, Castiglioni Pes and Co.) from Río Negro Province and an organic derivative (MMO), exchanged by hexadecyltrimethylammonium bromide provided by Fluka (Buchs, Switzerland). Briefly, the experiments were carried out in batch conditions (Volume= 25 mL, pH=6, temperature=25 ºC, contact time=24 h, solid/liquid relationship=3 g/L) varying the initial Pb concentration (100, 200, 300, 400, and 500 ppm) and the sorbent material (MMT and MMO). The Pb solutions were prepared by diluting a stock solution (Lead acetate trihydrate, $C_4H_6Pb{\cdot}3H_2O$, provided by Riedel-de Haën) with appropriate volumes of doubly–distilled water. Finally, the solid and liquid phases were separated by centrifugation (15000 rpm during 15 min). The liquid phases were disposed for the analysis of the remaining Pb elemental concentrations by LIBS and AAS techniques.

2.2 Experimental LIBS setup

The experimental setup employed for Pb determination by LIBS is shown in Fig. 1. It has been used previously for Mg and Cr determinations [27–29], so only a brief description is given here. A Nd:YAG laser operating at fundamental wavelength (Continuum Surelite II, λ=1064 Å, 7 ns pulse FWHM, 150 mJ/ pulse, repetition rate of 2 Hz) was used to generate the plasmas in air at atmospheric pressure on the samples, which were prepared in the form of pellets (Section 2.2). Each sample was mounted on a holder adjustable in x, y, z directions to allow for surface repositioning. During measurements, the sample rotates slowly to avoid the formation of a deep crater. The laser beam was focused at right angle onto the surface of the samples by means of a lens of 10 cm focal length. The lens–to–sample distance of this lens was lower than its focal length in such a way that the waist of the focused laser pulses was placed at a distance *d* below the sample surface by using a micrometer translation stage. The shape of the plasma plume was visualized during the experiment employing another lens to form a magnified lateral image of the plume on a screen (not shown in Fig. 1). Craters of about 0.15 mm^2 area were produced in the pellets by the laser shots. The resulting irradiance was about 10 GW/cm^2.

The spatially–integrated emission of the plasma was collected at right angles to the laser beam direction with a quartz lens of 20 cm focal length and focused into the entrance slit (100–μm–wide) of a monochromator (Jovin Yvon Czerny–Turner configuration, resolution 0.01 Å at λ=300 Å, focal length 1.5 m, grating of 2400 lines/mm). The detector was a photomultiplier (PM, Hamamatsu IP28, spectral response range 2000–6000 Å) whose signal was time resolved and averaged with a box–car. Finally, the spectra were recorded and processed by a PC. This experimental setup provided a high spectral resolution that allowed detailed measurements of individual line profiles of trace elements.

The measurements were performed with temporal resolution using suitable gate and delay times to discriminate the early plasma continuum from the late lines emission. The emission line profiles were scanned moving the diffraction grating of the monochromator controlled by software and synchronized with data acquisition and laser firing. To improve the signal–to–noise ratio, each experimental data point of the line profile was averaged for 3 laser shots and each spectral line was measured 3 times and further averaged. An accurate wavelength calibration was carried out with a standard Hg pencil lamp. The instrument profile was represented by a Gaussian function with a calculated full width at half maximum (FWHM) of 0.122 Å for the 100–μm width entrance/exit slits for a wavelength of 4000 Å.

Figure 1

2.3 LIBS analysis

The LIBS analysis was carried out at the spectroscopy laboratory of the IFAS Research Institute (Tandil, Argentina). The liquid samples were prepared for LIBS analysis in the form of pressed pellets by using the procedure reported previously [26]. Briefly, for each sample, 8 ml of liquid solution was employed and 6 g of powdered calcium oxide (CaO, Aldrich Chemistry 99.9%) added to form calcium hydroxide [$Ca(OH)_2$]. The mixture was well stirred and dried at room temperature in a place free of any possible contamination until constant weight was attained. The solid obtained was finely grinded, placed in a steel die, and pressed with a manual press at 20 Ton/cm^2 to form pellets of 3 cm of diameter and 1cm of thickness. For calibration purposes, 7 pellets with known Pb concentrations in the range 56–715 μg/g were prepared following the same procedure. It should be noted that the Pb concentration in the liquid samples, C_l

(μg/ml≡ppm), is related stoichiometrically to the corresponding Pb concentration in the pellets, C_p (μg/g), by

$$C_l = \frac{C_p.W}{V} \qquad (1)$$

where W (g) is the sample mass, and V (ml) the volume of the added solution.

2.4 AAS analysis

The AAS analysis was performed at the LAByM Laboratory (Tandil, Argentina). The determination of Pb in the liquid samples was performed by flame atomic absorption spectrometer (GBC 906, Australia) in air–acetylene flame under standard conditions [30]. The analyzer was calibrated by means of calibrations solutions prepared by diluting a stock solution with 100 ppm Pb. A linear calibration curve (R^2=0.999) was obtained with Pb concentrations ranging from 2.5 up to 20 ppm. The 5 analytical samples of each subset were properly diluted with bi–distilled water in a 4:20 v:v ratio and the corresponding absorbance values were measured to obtain the respective Pb concentrations. For each sample, two replicated measurements were carried out and further averaged to obtain its final Pb concentration.

3. Results and discussion

3.1 Optimization of LIBS measurements

The experimental conditions of measurement were optimized in order to improve the accuracy of the quantitative analysis. Quantitative information was obtained by relating the experimental results to the basic physics of a homogeneous plasma emission. This is difficult to be fulfilled in laser–induced plasmas in air because significant gradients of temperature exist. For this reason, a fixed focusing position of approximately d = 4 mm was kept during the whole experiment, selected by visual examination of the plasma image. For such an optimal value of d, a plasma with a maximum emission intensity for Pb and a more spherical shape were obtained, as already described by Aguilera et al. [31], and our previous works [27,28]. The emission coming from the brightest central region of the plume was measured by focusing it on the entrance slit of the monochromator. Table 1 shows the Pb I lines detected under our experimental conditions. These lines were recorded well isolated and free from interferences from other elements. Their spectroscopic parameters were obtained from NIST database [32]. The most intense Pb I line at 4057.78 Å was selected as the analytical line for calibrating the Pb content in the analyzed samples.

Table 1

Self–absorption effect in LIBS measurements has been widely discussed [33]. Self-absorption is determined by the optical thickness of the spectral lines. The optical thickness reaches its maximum value τ_0 at the line center and decreases toward the line wings. For low species concentration, self–absorption of radiation within the plasma is negligible, $\tau_0 << 1$, and the plasma is said to be optically thin. On the other hand, for high species concentration the radiation emitted has a large probability of being absorbed, then $\tau_0 >> 1$, and the plasma is said to be optically thick. In this latter case, the line peak intensity saturate at a value given by the Plank blackbody distribution. Hence, the corresponding calibration curve bends for relatively higher concentrations. Thus, the sensitivity of the curve decreases and the measured line intensity is not proportional to the element concentration in the sample. Different methods have

been reported aimed to evaluate and compensate self–absorption of spectral lines taking place inside the plasma (see [34] and refs. therein). Nevertheless, they result intrinsically more elaborated and time–consuming. Alternatively, self–absorption of spectral lines can be overcome or reduced by a proper selection of the conditions of measurement, mainly the observing time window after the laser ablation [35, 36]. Thus, experimental working conditions of negligible self–absorption of Pb I lines in the plasma were determined by means of a study of the temporal evolution of the Pb I emission intensity and the continuum signal.

Fig. 2 shows the temporal behavior of the peak intensity of the Pb I line at 4057.8 Å and the continuum in the vicinity of the line at 4057.0 Å, measured from the calibration sample having the highest Pb concentration. It is observed that the dynamics of Pb I emission and the continuum, due to bremsstrahlung radiation and radiative recombination, are very different and they depend critically on the observing time after the laser ablation (i.e: delay time). Initially, for delay times $\leq$ 10 μs, the Pb I emission was superimposed to an intense continuum due to the high electronic density of the plasma. After that, the continuum intensity decreased quickly with time and the Pb I emission appeared, it raised to reach a maximum value between 15 and 25 μs, and then it decreased due to plasma cooling at about 70 μs. A similar behavior was observed for the sample with lower Pb contents but with minor intensities.

The calculated signal–to–background–ratio (SBR) is also displayed in Fig. 2. The SBR suffered a rapid increment at initial times due to the drop of the continuum, stabilized at middle times, and decreased at later times due to the relatively weak line emission. An adequate selection of the measurement time window (delay time, t_d , and gate time, t_g) involved a tradeoff between high values for both, line intensity and SBR, together with a negligible self–absorption. In Fig. 2, the highest Pb I peak intensity is observed in the time interval 15–27 μs with an approximately constant value. This can be probably due to a strong self–absorption of the Pb I line as a result of a high density of species present in the plume at those instants of its evolution. After that, the emission intensity decreased steadily, indicating that self–absorption effects diminished. In addition, the SBR ratio remained approximately constant from 15 μs up to 45 μs. Thus, a time window of 30–45 μs (i.e.: t_d = 30 μs; t_g = 15 μs) was selected for the LIBS analysis where suitable conditions for a good sensitivity of the calibration curve in the concentration range of interest and avoiding possible self–absorption effects were attained, as will be shown in Section 3.3. Moreover, since the Pb I line at 4057.8 Å was the most intense line measured under our selected experimental, we can infer that the other relatively weaker Pb I lines were also emitted in optically thin conditions. Pb II lines were not detected at this time interval due to recombination of the plasma.

Figure 2

3.2 Plasma characterization

The determination of the plasma parameters is very important to obtain the LTE condition which is critical for the quantitative analysis. The LIBS plasma was characterized with the measured Pb I emission lines (Table 1) through the determination of the temperature and the electron number density, assuming that the plasma was close to LTE. This assumption is based in the fact that LTE is generally fulfilled in LIBS experiments by the relatively high electron densities achieved in the plasma [37]. The emission profiles of the Pb I lines were measured from the standard sample with the highest Pb content. The experimental lines (corrected for the quantum efficiency of the PM) were fitted to Voigt profiles with a Gaussian width, w_G=0.123Å, associated to the quadratic combination of the instrumental width, w_{Instr}=0.122 Å, plus the Doppler width, $w_{Doppler}$=0.015Å, estimated from the plasma temperature, while the Lorentzian width was related to the Stark broadening, w_{Stark}. The Gaussian width was fixed while the Stark width was a free fitting parameter. The net intensities were given by the integrated area of the

line profile subtracting the background baseline. The temperature of the plasma was determined from a Boltzmann plot constructed with the net emission intensities of Pb I lines, from which a value of T = (5800 ± 1160) K for ΔE= 1.8 eV was obtained (Fig. 3). The error was estimated from the propagation of the error in determining the slope value from the linear fitting.

The electron density N_e (cm^{-3}) was calculated from the Stark broadening of the Pb I line at 4057.8 Å. In typical LIBS experiences, Stark broadening is the predominant mechanism that determines the Lorentzian contribution to the line profile [38]. It is proportional to the electron number density, namely,

$$w_{Stark} = 2w_p \frac{N_e}{N_e^{Ref}} \qquad (2)$$

where w_{Stark} (Å) is the Stark width (FWHM) of the transition considered at the electron density N_e (cm^{-3}), w_p is the Stark broadening parameter (HWHM), and N_e^{Ref} (cm^{-3}) is a reference electron density, usually 10^{16} or 10^{17} cm^{-3}, at which the parameter w_p was measured or calculated [37]. The Pb I line at 4057.8 Å was recorded with a high SBR suitable for an accurate calculation of the electron density. In order to increase the accuracy of w_{Stark} measurement, the slit width of the monochromator was reduced down to 50 μm in order to decrease the instrumental contribution to the line width. Hence, the Stark broadening obtained for this transition was w_{Stark} = (0.063 ± 0.002) Å, which was of the same order than the instrumental width, w_{Instr} = 0.061 Å for the 50–μm width entrance/exit slits (λ = 4000 Å). The electron density was obtained by comparing our measured Stark width with the value reported for the same line by Alonso–Medina [39], normalized to an electron density of 10^{17} cm^{-3} for a plasma temperature of 11200 K, considering that the error due to the difference of temperature is small taking into account that w_p is a parameter weakly dependent on the temperature [35]. The calculated electron density was N_e = (4.5 ± 0.1) x10^{16} cm^{-3}. The error was estimated from the fitting error of the measured w_{Stark}.

A criterion proposed by McWhirter [40] necessary to satisfy LTE conditions in a plasma medium is based on a lower limit to the electron density for which the collisions with electrons dominate over the radiative processes. The critical electron density, N_e^0 (cm^{-3}), is

$$N_e^0 = 1.6x10^{12}\, T^{1/2}\, \Delta E^3 \qquad (3)$$

Here, T (K) is the plasma temperature and ΔE (eV) is the energy gap difference between the transition levels. The critical electron number density calculated with Eq.(3) was N_e^0 = 7.1x10^{14} cm^{-3}, which is about two orders of magnitude lower than that determined in our experiment. McWhirter's criterion is a necessary but not sufficient to assure LTE; however, no additional measurements were carried out and LTE condition was assumed [15]. It should be stressed that the temperature and electron density values calculated here have been derived via time– and spatial–integrated spectra. Thus, they corresponded to apparent values due to population–averaging over the real spatial–temporal distribution of species emissivity along the line of observation, as described in [41].

Figure 3

3.3 Analysis of Pb sorption

Quantitative determination of the remaining Pb content in the MMT–treated water solutions was performed by LIBS with the calibration curve method. The line profiles of the Pb I line at 4057.8 Å were recorded from the different standard samples (Fig. 4). A calibration curve was constructed by plotting the measured net intensities versus the corresponding Pb concentrations

(Fig. 5). The experimental data showed a linear trend with a good sensitivity and a negligible self–absorption for the measured concentration range (56–715 μg/g). The data were fitted to a straight line (R^2=0.914). The error bars corresponded to the standard deviations from the different measurement of the line profiles. The Pb concentrations (μg/g) in the analytical samples were determined by interpolation in the linear fit function and the concentrations in the liquid solutions (ppm) were calculated by means of Eq. (1).

Figure 4

Figure 5

The results for the remaining Pb concentrations in the liquid solutions determined with LIBS and AAS are exposed in Table 2. It should be mentioned that in the MMT 100 sample the Pb I emission signal was not detected with LIBS in our experimental conditions. This means that the actual Pb concentration was below the detection limit (*LoD*), which is defined as the minimum detectable concentration [42]. In this work, the *LoD* was not calculated since it required the measurement of a calibration curve with Pb concentrations in the range of a few ppm. Nevertheless, we can take as a reference value *LoD* = 20 ppm, given for Pb in our previous work [26].

In Fig. 6, the LIBS results for water solution after treatment with MMT and MMO clays are compared. It is observed that the measured Pb concentration was lower than the initial concentration due to its incorporation into the MMT clays. Moreover, the remaining Pb concentrations were lower for MMT than for MMO, indicating a higher sorption in the first case. A sorption percentage S_{Pb}% was employed to calculate the sorption efficiency on Pb–contaminated water. It was calculated as

$$S_{Pb}\% = \frac{c_i - c_f}{c_i}.100 \qquad (4)$$

where c_i, c_f (ppm) are the initial and final Pb concentrations, respectively. The calculated S_{Pb}% against the initial Pb concentrations are shown in Fig. 7. In both cases, the calculated S_{Pb}% showed a linear decrease with the initial Pb content, while it was higher for MMT (56%–100%) than for MMO (27%–47%). The different slope values denote the different sorption features of the two kinds of clays. MMT sorbed more Pb than MMO due to their differences in the superficial net charge of the materials. Raw montmorillonite is more negative than organic one and, therefore, there exists stronger electrostatic interaction between natural clay and Pb than organic clay and the metal.

Table 2

Figure 6

In order to validate the LIBS results, they were compared with the Pb concentrations obtained with AAS (Fig. 8). The averaged quantification error was evaluated through a normalized standard deviation σ_N %, calculated as

$$\sigma_N\% = \sqrt{\frac{\sum[(q_{LIBS} - q_{AAS})/q_{LIBS}]^2}{n-1}}.100 \qquad (5)$$

where q_{LIBS} and q_{AAS} refer to the calculated values with LIBS and AAS techniques, respectively, and n is the number of samples (i.e.: n=10). A value of σ_N % = 16.5 % was obtained for all the samples analyzed which indicated that the compositional results obtained by LIBS were in a very good agreement with those obtained by AAS.

Figure 7

Figure 8

4. Conclusions

LIBS technique was successfully applied for the quantitative determination of Pb elemental concentration in residual water solutions treated with MMT clay for heavy metal removal. Optimal measurement conditions for LIBS method were found in order to obtain reliable analytical results. The laser–induced plasma was characterized through the calculus of the temperature and the electron density.

The sorption efficiency of raw MMT and MMO clays were assessed by quantification of the remaining Pb concentration in analytical water solutions through a calibration curve constructed with the Pb I line at 4057.8 Å. The calculated sorption percentages of Pb were higher for raw MMT (56%–100%) than for MMO (27%–47%). A good agreement were found between the results obtained by LIBS technique and the conventional analytical technique AAS. Overall, these results contributed to the investigation of heavy metal sorption by MMT clay. In the future, this research will be extended to other elements, such as Co, Zn, Cs, and Sr, which are of environmental relevance.

Acknowledgments

This work was supported by Consejo Nacional de Investigaciones Científicas y Técnicas (CONICET), and Comisión de Investigaciones Científicas de la Provincia de Buenos Aires (CICPBA).

References

[1] R. Renner, Exposure on tap: drinking water as an overlooked source of lead, Environ. Health Perspect. 118 (2010) A68–72.

[2] M.D. Giripunje, A.B. Fulke, P.U. Meshram, Remediation techniques for heavy-metals contamination in lakes: a mini-review, Clean—Soil Air Water 43 (2015) 1350–1354.

[3] L. Järup, Hazards of heavy metal contamination, Brit. Med. Bull. 68 (2003) 167–182.

[4] R. Zhu, Q. Chen, Q. Zhou, Y. Xi, J. Zhu, H He, Adsorbents based on montmorillonite for contaminant removal from water: a review, Appl. Clay Sci. 123 (2016) 239–58.

[5] S.S. Gupta, K.G. Bhattacharyya, Adsorption of heavy metals on kaolinite and montmorillonite: a review, Phys. Chem. Chem. Phys. 14 (2012) 6698–723.

[6] F.M. Flores, T. Undabeytia, E. Morillo, R.M. Torres Sánchez, Pyrimethanil adsorption/desorption on montmorillonite and organo-montmorillonites: flocculation assays for technological application in fruit packing plants wastewater, Environ. Sci. and Pollution Res. 24 (2017) 14463-14476.

[7] A.V. Gil Rebaza, M.L. Montes, M.A. Taylor, L.A. Errico, R.E. Alonso, Experimental and theoretical study of Co sorption in clay montmorillonites, Mater. Res. Express 5 (2018) 035519.

[8] J.D.Winefordner, I.B. Gornushkin, T. Correll, E. Gibb, B.W. Smith, N. Omenetto, Comparing several atomic spectrometric methods to the super stars: special emphasis on laser induced breakdown spectrometry, LIBS, a future super star, J. Anal. At. Spectrom. 19 (2004) 1061–1083.

[9] R.S. Harmon, R.E. Russo, R.R. Hark, Applications of laser–induced breakdown spectroscopy for geochemical and environmental analysis: a comprehensive review, Spectrochim. Acta Part B 87 (2013) 11–26.

[10] A.W. Miziolek, V. Palleschi, I. Schechter, Laser induced breakdown spectroscopy, Cambridge University Press, Cambridge, 2006.

[11] D.A. Cremers, L.J. Radziemski, Handbook of laser–induced breakdown spectroscopy, Wiley, Chichester, 2006.

[12] J.P. Singh, S.N. Thakur, Laser–induced breakdown spectroscopy, Elsevier, Amsterdam, 2007.

[13] C. Pasquini, J. Cortez, L.M.C. Silva, F.B. Gonzaga, Laser induced breakdown spectroscopy, J. Braz. Chem. Soc. 18 (2007) 463–512.

[14] E. Tognoni, V. Palleschi, M. Corsi, G. Cristoforetti, N. Omenetto, I. Gornushkin, B.W. Smith, J.D. Winefordner, From sample to signal in laser–induced breakdown spectroscopy: a complex route to quantitative analysis, in: A.W. Miziolek, V. Palleschi, I. Schechter (Eds.), Laser–induced Breakdown Spectroscopy (LIBS) Fundamentals and Applications, Cambridge University Press, New York, 2006, pp. 122–170.

[15] D.W. Hahn, N. Omenetto, Laser–induced breakdown spectroscopy (LIBS), part I: review of basic diagnostics and plasma–particle interactions: still–challenging issues within the analytical plasma community, Appl. Spectrosc. 64 (2010) 335A–366A.

[16] D.W. Hahn, N. Omenetto, Laser–Induced Breakdown Spectroscopy (LIBS), part II: review of instrumental and methodological approaches to material analysis and applications to different fields, Appl. Spectrosc. 66 (2012) 347–419.

[17] R.S. Harmon, R.E. Russo, R.R. Hark, Applications of laser–induced breakdown spectroscopy for geochemical and environmental analysis: A comprehensive review, Spectrochim. Acta Part B 87 (2013) 11–26.

[18] D.A. Cremers, L.J. Radziemski, T.T. Loree, Spectrochemical analysis of liquids using the laser spark, Appl. Spectrosc. 38 (1984) 721–729.

[19] G. Arca, A. Ciucci, V. Palleschi, S. Rastelli, E. Tognoni, Trace element analysis in water by laser–induced breakdown spectroscopy technique, Appl. Spectrosc. 51 (1997) 1102.

[20] L. St–Onge, E. Kwong, M. Sabsabi, E.B. Vadas, Rapid analysis of liquid formulations containing sodium chloride using laser–induced breakdown spectroscopy, J. Pharm. Biomed. Anal. 36 (2004) 277–284.

[21] J.O. Cáceres, J. Tornero López, H.H. Telle, A. González Ureña, Quantitative analysis of trace metals ions in ice using laser–induced breakdown spectroscopy, Spectrochim. Acta Part B 56 (2001) 831–838.

[22] F. Borges, J. Uzuriaga Ospina, G. Cavalcanti, E.E. Farias, A. Araujo Rocha, P.I.L.B. Ferreira, G. Cerqueira Gome, A. Mello. CF–LIBS analysis of frozen aqueous solution samples by using a standard internal reference and correcting the self–absorption effect, J. Anal. At. Spectrom. 33 (2018) 629–641.

[23] R.L. Vander Wal, T.M. Ticich, H.R. West Jr., P.A. Householder, Trace metal detection by laser–induced breakdown spectroscopy, Appl. Spectrosc. 53 (1999) 1226–1235.

[24] S.T. Järvinen, J. Saarela, J. Toivonen, Detection of zinc and lead in water using evaporative preconcentration and single–particle laser–induced breakdown Spectroscopy, Spectrochim. Acta Part B 86 (2013) 55–59.

[25] S. Niu, L. Zheng, A.Q. Khan, G. Feng, H. Zeng, Laser–induced breakdown spectroscopic detection of trace level heavy metal in solutions on a laser–pretreated metallic target, Talanta 179 (2018) 312–317.

[26] D.M. Díaz Pace, C.A. D'Angelo, D. Bertuccelli, G. Bertuccelli, Analysis of heavy metals in liquids using Laser Induced Breakdown Spectroscopy by liquid–to–solid matrix conversion, Spectrochim. Acta Part B 61, 929–933 (2006).

[27] D.M. Díaz Pace, C.A. D'Angelo, G. Bertuccelli. Calculation of optical thicknesses of magnesium emission spectral lines for diagnostics of laser induced plasmas, Appl. Spectrosc. 65 (2011) 1202–1212.

[28] D.M. Díaz Pace, C.A. D'Angelo, G. Bertuccelli, Study of self–absorption of emission magnesium lines in laser–induced plasmas on calcium hydroxide matrix, IEEE Trans. Plasma Sci. 40 (2012) 898–908.

[29] D.M. Díaz Pace, Laser–induced plasma characterization using line profile analysis of chromium neutral atom and ion transitions, J. Quant. Spectrosc. Radiat. Transfer 129 (2013) 254–262.

[30] Standard methods for the examination of water and wastewater, American Public Health Association, Washington DC, 2012, pp. 16-17.

[31] J.A. Aguilera, J. Bengoechea, and C. Aragón, Spatial characterization of laser induced plasmas obtained in air and argon with different laser focusing distances, Spectrochim. Acta Part B 59 (2004) 461–469.

[32] NIST Atomic Spectra Database. https://www.nist.gov/pml/atomic-spectra-database, 2017 (accessed 15 April 2017).

[33] C. Aragón, J. Bengoechea, J.A. Aguilera, Influence of the optical depth on spectral line emission from laser–induced plasmas, Spectrochim. Acta Part B, 56 (2001) 619–628.

[34] Cristoforetti G, Tognoni E, Calculation of elemental columnar density from self–absorbed lines in laser–induced breakdown spectroscopy: a resource for quantitative analysis, Spectrochim. Acta Part B 79–80 (2013) 63–71.

[35] J.A. Aguilera, C. Aragón, Characterization of laser–induced plasmas by emission spectroscopy with curve–of–growth measurements. Part I: Temporal evolution of plasma parameters and self–absorption, Spectrochim. Acta Part B 63 (2008) 784–792.

[36] J.A. Aguilera, C. Aragón C, Characterization of laser–induced plasmas by emission spectroscopy with curve–of–growth measurements. Part II: Effect of the focusing distance and the pulse energy, Spectrochim. Acta Part B 63 (2008) 793–799.

[37] C. Aragón , J.A. Aguilera, Characterization of laser induced plasmas by optical emission spectroscopy: a review of experiments and methods, Spectrochim. Acta Part B 63 (2008) 893–916.

[38] H.R. Griem, Plasma spectroscopy, McGraw–Hill, New York, 1964.

[39] A. Alonso–Medina, Experimental determination of the Stark widths of Pb I spectral lines in a laser–induced plasma, Spectrochim. Acta Part B 63 (2008) 598–602.

[40] R.W.P. McWhirter, in: R.H. Huddlestone, S.L. Leonard (Eds.), Plasma Diagnostic Techniques, Academic Press, New York 1965, pp. 201–264 (Chapter 5).

[41] J.A. Aguilera, C. Aragón, Characterization of a laser–induced plasma by spatially resolved spectroscopy of neutral atom and ion emissions. Comparison of local and spatially integrated measurements, Spectrochim. Acta B 59 (2004) 1861–1876.

[42] M. Sabsabi, P. Cielo, Quantitative analysis of aluminum alloys by laser induced breakdown spectroscopy and plasma characterization, Appl. Spec. 49 (1995) 499–507.

Tables

Table 1. Pb I lines used for plasma characterization. Data from Ref.[32].

Species	Wavelength (Å)	A_{ji} (s^{-1})	E_j (eV)	E_i (eV)	g_j	g_i
Pb I	283.30	4.90×10^7	4.37	0.00	3	1
Pb I	357.27	9.90×10^7	6.13	2.66	3	5
Pb I	368.34	1.37×10^8	4.33	0.97	1	3
Pb I	373.99	7.30×10^7	5.97	2.66	5	5
Pb I	405.78[a]	9.00×10^7	4.37	1.32	3	5

[a] Analitical line selected for quantitative determination of Pb.
A_{ji} (s^{-1}) is the transition probability; E_j, E_i (eV) are the energies of the lower and upper energy levels; g_j, g_i (dimensionless) are the degeneracies of the levels.

Table 2. Remaining Pb concentrations determined with LIBS and AAS for the water solutions treated with raw (MMT) and organic (MMO) montmorillonite clays.

Samples	Initial Pb concentration (ppm)	Remaining Pb concentration (ppm)	
		LIBS[#]	AAS[§]
Natural Montmorillonite			
MMT 100	100	*< 20* ± 4	2.00 ± 0.01
MMT 200	200	28 ± 6	26.00 ± 1.40
MMT 300	300	50 ± 8	59.00 ± 1.81
MMT 400	400	157 ± 16	115.00 ± 2.99
MMT 500	500	211 ± 23	177.00 ± 4.63
Organic Montmorillonite			
MMO 100	100	53 ± 12	38.00 ± 2.02
MMO 200	200	117 ± 15	101.00 ± 3.01
MMO 300	300	169 ± 18	188.00 ± 0.57
MMO 400	400	255 ± 24	247.00 ± 1.61
MMO 500	500	367 ± 28	373.00 ± 12.87

[#] Limit of detection for LIBS: 20 ppm, taken from Ref. [26].
[§] Limit of detection for AA: 0.015 ppm, taken from Ref. [30].

Figures

Fig. 1

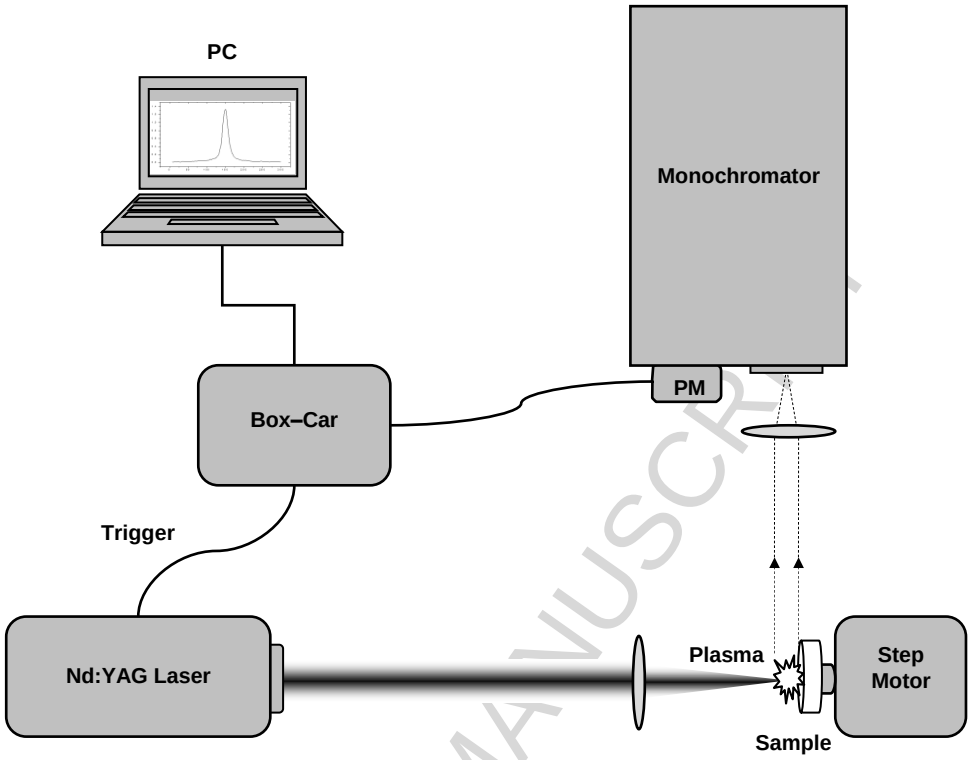

Fig. 2

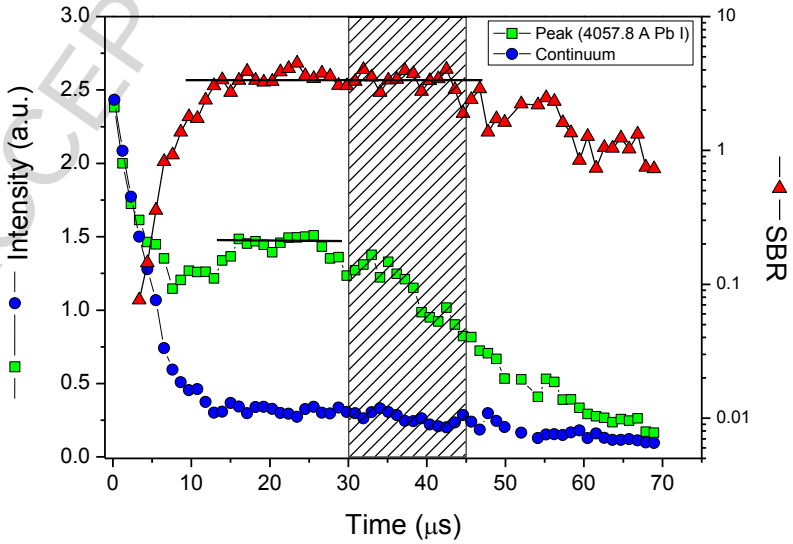

Fig. 3

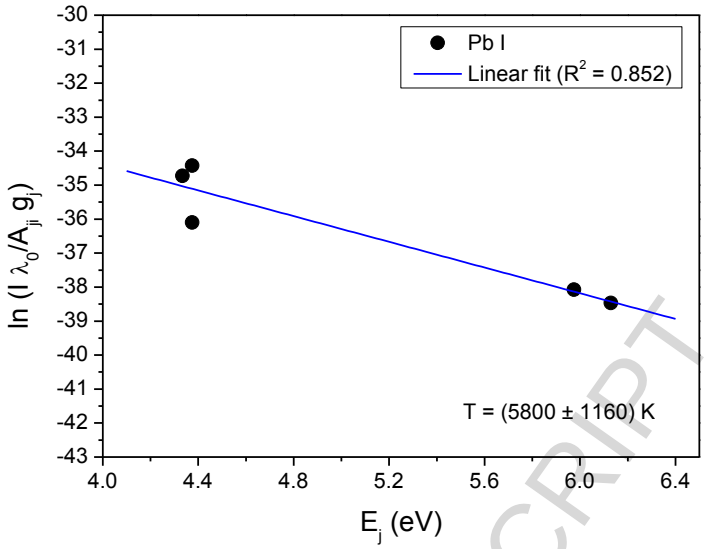

Fig. 4

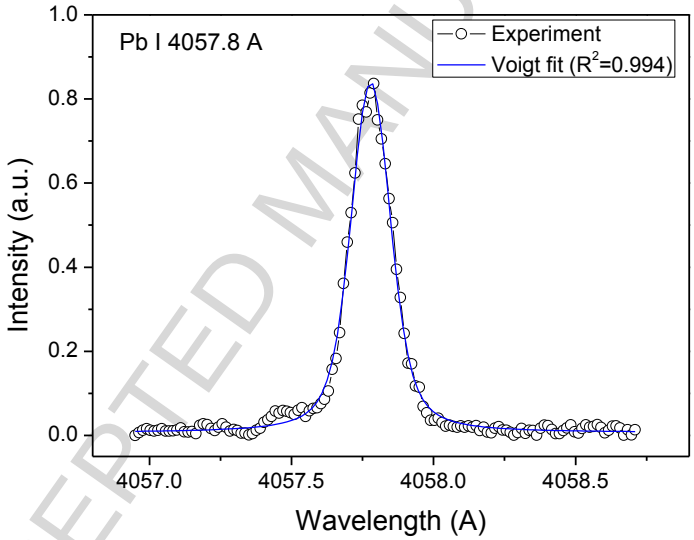

Fig. 5

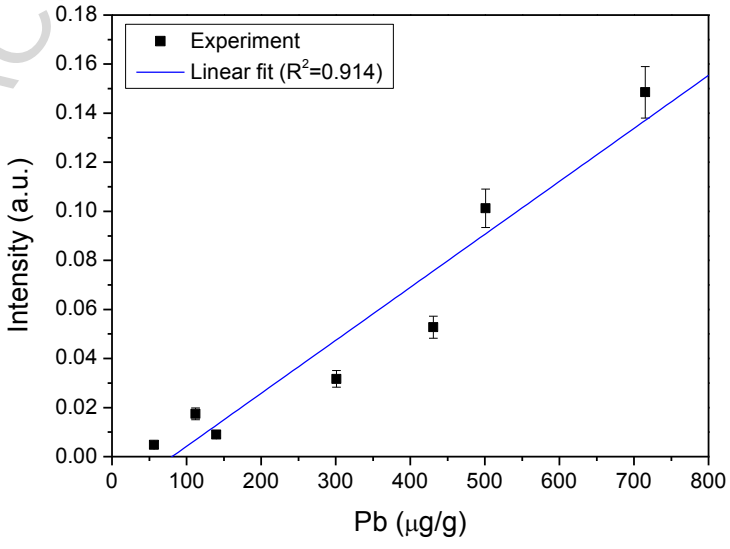

Fig. 6

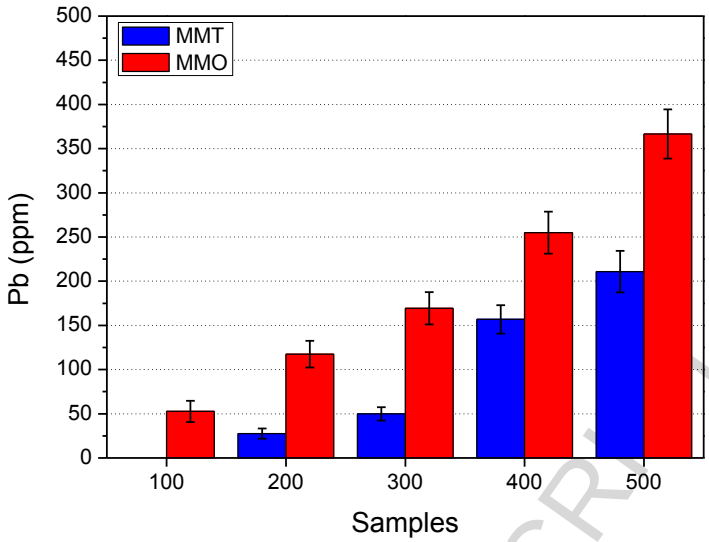

Fig. 7

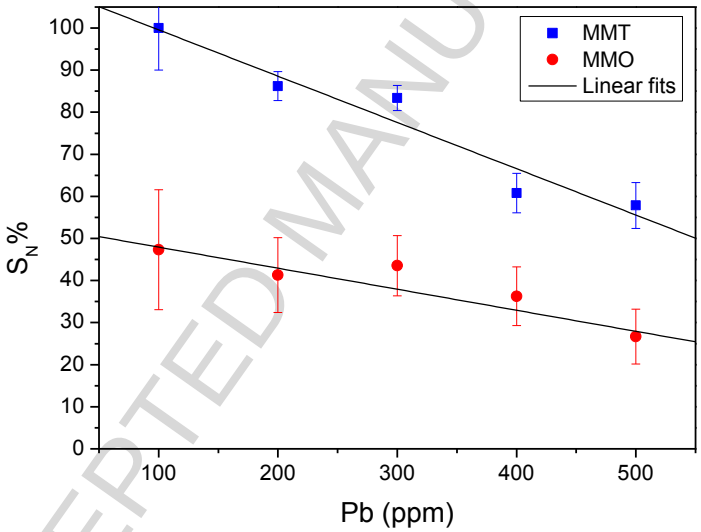

Fig. 8

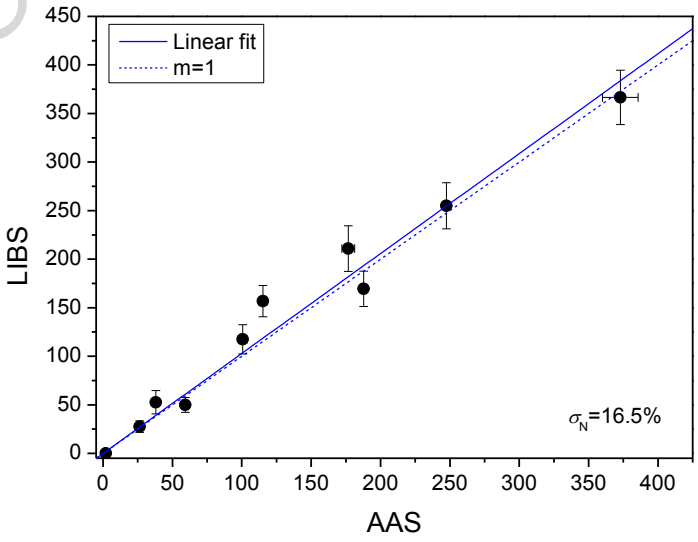

Figure captions

Fig. 1. Experimental setup used for LIBS measurements.

Fig. 2. Time evolution of the peak emission of Pb I line at 4057.8 Å (□), the continuous background close to the line (○), and the calculated signal–to–background ratio, SBR (△). The measurement time window is indicated. (Note the logarithm scale on right y–axis).

Fig. 3. Boltzmann plot constructed with spatially–integrated optically thin intensities of Pb I lines of Table 1.

Fig. 4. Example of experimental and fitting profiles of the Pb I line at 4057.8 Å from the pellet with 715 μg/g Pb.

Fig. 5. LIBS calibration curve for Pb.

Fig. 6. Remaining Pb concentrations obtained with LIBS for the different liquid solutions (x–axis) treated with raw (MMT) and organic (MMO) montmorillonite clays.

Fig. 7. Sorption percentages (S_N%) calculated for raw (MMT) and organic (MMO) montmorillonite clays for different initial Pb concentrations (x–axis).

Fig. 8. Comparison of LIBS and AAS results. The calculated averaged quantification error (σ_N%) is shown. The dotted line corresponds to the ideal situation (m=1).

Highlights

- Treatment of water samples with raw montmorillonite and organic derivative clays.
- Quantitative analysis of remaining Pb content via Laser–induced breakdown spectroscopy (LIBS) and atomic absorption spectroscopy (AAS) techniques.
- Calculation of the sorption percentages.
- LIBS technique can provide an accurate determination of residual Pb in water samples.